Atmos. Meas. Tech., 19, 5267–5280, 2026
https://doi.org/10.5194/amt-19-5267-2026
© Author(s) 2026. This work is distributed under
the Creative Commons Attribution 4.0 License.

Atmospheric Measurement Techniques
Open Access
EGU

An absolute reference frame for nitrous oxide clumped and position-specific isotopes provided by thermal equilibration

Paul M. Magyar[1], Nico Kueter[2,3], Simone Brunamonti[1], Naizhong Zhang[1], Ivan Prokhorov[1], Noémy Chénier[1,4], Lukas Emmenegger[1], Béla Tuzson[1], and Joachim Mohn[1]

[1]Empa, Laboratory for Air Pollution/Environmental Technology, 8600 Dübendorf, Switzerland
[2]Department of Earth and Planetary Sciences, ETH Zürich, 8092 Zurich, Switzerland
[3]Geological Institute, RWTH Aachen University, 52062 Aachen, Germany
[4]Department of Environmental Science, University of Basel, 4056 Basel, Switzerland

Correspondence: Paul M. Magyar (paul.magyar@empa.ch)

Received: 13 February 2026 – Discussion started: 31 March 2026
Revised: 17 July 2026 – Accepted: 18 July 2026 – Published: 12 August 2026

Abstract. Clumped isotopic measurements of nitrous oxide (N_2O) have the potential to offer unique constraints on the processes governing N_2O production and destruction, building on the information provided by $\delta^{15}N$, $\delta^{18}O$ and ^{15}N site preference (SP). Extending their application requires a robust absolute reference frame. Here we show that thermal equilibration of N_2O over γ-Al_2O_3 provides such a reference frame for measurements of the isotopologues $^{14}N^{15}N^{18}O$ and $^{15}N^{14}N^{18}O$, as well as for SP. Using a quantum cascade laser absorption spectroscopy (QCLAS) platform, we simultaneously quantify seven isotopologues of N_2O, including $^{14}N^{15}N^{18}O$, $^{15}N^{14}N^{18}O$, and $^{15}N^{15}N^{16}O$. Experiments starting from isotopically-distinct starting materials show convergence to time-invariant compositions that are in agreement with theoretically predicted temperature dependencies. These results demonstrate that γ-Al_2O_3 activated at $\geq 550\,°C$ catalyzes isotope exchange among isotopologues of N_2O at equilibration temperatures between 153 and 218 °C and thereby define an absolute stochastic reference frame for $\Delta^{14}N^{15}N^{18}O$ and $\Delta^{15}N^{14}N^{18}O$. In contrast, $^{15}N^{15}N^{16}O$ does not equilibrate under these conditions, suggesting selective activation of N–O but not N–N bonds. Comparison of equilibrium SP values with theoretical predictions reveals a systematic offset relative to the current reference scale, which will require future work to reconcile.

1 Introduction

Nitrous oxide (N_2O) is a significant anthropogenically-stimulated greenhouse gas and ozone depleting molecule (Tian et al., 2020; Yu et al., 2020). Mitigation of its emissions is strongly supported by identifying environmental or physiological variations in nitrous oxide production and consumption. The clumped isotopologues $^{14}N^{15}N^{18}O$, $^{15}N^{14}N^{18}O$, and $^{15}N^{15}N^{16}O$ show promise as new constraints on these variations, building on the information already available from position-specific and bulk isotopic measurements of N_2O (Kantnerová et al., 2020b, 2022; Magyar et al., 2016; Magyar, 2017; Ostrom and Ostrom, 2017). Two methods have been reported for accurate and precise quantification of these rare clumped isotopologues: high-resolution isotope-ratio mass spectrometry (HR-IRMS) and quantum cascade laser absorption spectroscopy (QCLAS). HR-IRMS utilizes measurements of $^{14}N^{15}N^{18}O + {}^{15}N^{14}N^{18}O$ and the fragment $^{15}N^{18}O$ to quantify $^{14}N^{15}N^{18}O$ and $^{15}N^{14}N^{18}O$, but requires significant and variable background and rearrangement corrections and long measurement times of $\geq 8\,h$ per sample (Kantnerová et al., 2020a; Magyar et al., 2016). QCLAS enables direct measurements of $^{14}N^{15}N^{18}O$ and $^{15}N^{14}N^{18}O$, as well as $^{15}N^{15}N^{16}O$ (Kantnerová et al., 2020a), but is subject to drift effects and therefore requires relatively fast measurement cycles to take advantage of its intrinsic selectivity and sensitivity (Gonzalez et al., 2019; Nataraj et al., 2022; Tuzson et al., 2008; Waechter et al., 2008; Werle, 2011). This method uses a dual-laser spectrometer to simultane-

ously quantify three clumped and four singly-substituted stable isotopic constraints and – as long as instrument stability can be assured and fast measurement enabled – appears to be a superior approach for measuring rare N_2O isotopologues (Kantnerová et al., 2020a).

Any approach to measuring the clumped isotopic composition of N_2O requires a reliable reference frame. Clumped isotopes offer a specific advantage because their abundances are directly related to thermodynamically-calculable equilibrium constants (Eiler and Schauble, 2004; Urey and Rittenberg, 1933). This has been used to provide absolute reference frames for clumped isotopic measurements of carbonate minerals, methane, and other molecules (Bernasconi et al., 2018; Stolper et al., 2014). For N_2O, the full equilibrium composition of all twelve isotopologues can be described by a system of eight reactions, each with an associated equilibrium constant, as detailed by Wang et al. (2004). One of these reactions, Reaction (R1), is directly connected to ^{15}N site preference (SP), and so its variation with temperature at equilibrium can also be predicted (Bigeleisen and Friedman, 1950; Cao and Liu, 2012; Wang et al., 2004; Webb and Miller, 2014).

$$^{15}N^{14}N^{16}O \rightleftharpoons {}^{14}N^{15}N^{16}O \quad \text{(R1)}$$

To date, however, such variations have not been used as a reference for N_2O SP measurements.

The utility of isotope exchange reactions as a reference frame comes not just from the ability to predict but also to experimentally generate equilibrium distributions of isotopes among isotopologues. Unlike CO_2, N_2O cannot readily be brought to an equilibrium isotopic composition by heating alone, as thermal decomposition outpaces equilibrium exchange reactions. However, activated alumina has been identified as a catalyst for driving isotope exchange reactions for $^{14}N^{15}N^{18}O$, $^{15}N^{14}N^{18}O$, and SP (Kantnerová et al., 2020a; Magyar et al., 2016). In subsequent years, the γ phase of alumina (γ-Al_2O_3) was also identified as a catalyst for the equilibration of methane clumped isotopologues (Eldridge et al., 2019, 2023; Turner et al., 2021; Wang et al., 2020a). Since activated alumina represents a poorly defined mixture of various Al_2O_3 phases including γ-Al_2O_3, we anticipate that γ-Al_2O_3 is also a suitable material for the catalytic activation of N_2O. For methane, γ-Al_2O_3 is activated under vacuum at 567 °C before its use as a catalyst (Eldridge et al., 2019; Robertson et al., 1975). Such activation is likely related to desorption phenomena and surface structural transformations that occur in Al_2O_3 phases before the conversion to α-Al_2O_3 at higher temperatures (Cancellieri et al., 2024; Gramatte et al., 2023; Prins, 2020).

Here, we report the clumped and position-specific isotopic composition of nitrous oxide heated in the presence of γ-Al_2O_3 to drive it towards predicted equilibria. We evaluate the equilibrium nature of these reactions by demonstrating a common, time-invariant isotopic composition matching theoretical predictions for different starting materials, and assess the effect of thermal decomposition as compared to putative equilibrium reactions. We establish conditions for preheating γ-Al_2O_3 to activate its catalytic activity for driving internal isotopic equilibrium reactions. To accomplish these measurements and provide a basis for future applications of N_2O clumped isotope measurements, we made improvements to the temperature stability and sample introduction for the QCLAS platform. Finally, we establish an absolute reference frame for the parameters $\Delta^{14}N^{15}N^{18}O$ and $\Delta^{15}N^{14}N^{18}O$ and discuss implications for measurements and interlaboratory comparisons of ^{15}N site preference. We expect that our findings will facilitate application of isotopic tools to better constrain natural and anthropogenic source and sink processes for atmospheric N_2O and to monitor ambient N_2O in background air.

2 Methods

2.1 Laser spectroscopy

To measure the seven-dimensional isotopic composition of N_2O, we used an updated version of the QCLAS platform described by Kantnerová et al. (2020a). This instrument consists of a dual-laser spectrometer (QC-TILDAS-DUAL, Aerodyne Research Inc., USA) with quantum cascade laser sources emitting at 2142 and 2182 cm^{-1} to quantify the eight most abundant isotopologues of N_2O, as shown in Fig. 1. We implemented an astigmatic Herriott multipass cell (AMAC-36LW, Aerodyne Research Inc.) with 36 m optical path length in 350 mL volume to replace the cell (210 m, 2500 mL) originally installed in this instrument (Kantnerová et al., 2020a). This smaller cell improves signal-to-noise, normalized to the sample amount, by substantially reducing the light loss upon reflection and by lowering the interference fringe level. It also enables faster sample gas extraction and sample-reference exchange time. To compensate for the shorter path length, we measure samples as mixtures of $\sim$ 8 % N_2O in N_2, instead of the $\sim$ 1.65 % mixtures used previously. At a typical working pressure of 4.8 hPa, $\sim$ 4 µmol of N_2O are introduced into the multipass cell for each measurement cycle. To reduce the effects of temperature, the QCLAS was housed in a temperature-controlled plexiglass box (InduTec 400, Elinter, Switzerland), supplementing the temperature regulation of the spectrometer (ThermoRack 401, Solid State Cooling, USA). As a net result, variations in the laboratory temperature of $\pm$0.5 K are dampened to $\pm$20 mK in the outer box and $\pm$5 mK or better at the spectrometer cell. This level of temperature stability is necessary to achieve the required measurement precision (Bajnai and Hare, 2025).

To enable fast cycling between samples and reference materials, a customized gas inlet system was constructed (Fig. 1), similar to those described previously (Hare et al., 2022; Wang et al., 2020b; Zhang et al., 2025). This system consists of pneumatic valves (Swagelok, USA) connected

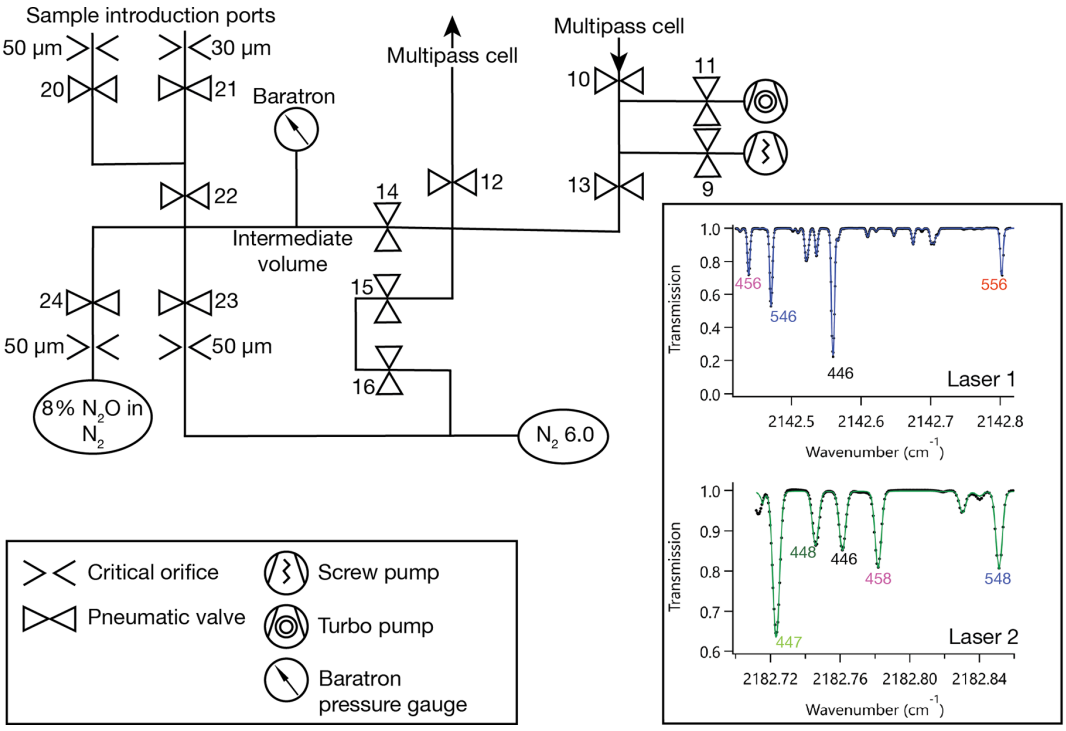

Figure 1. Schematic of the inlet system. Samples are introduced through critical orifices at valves 20 or 21 and mixed with N_2 in the intermediate volume between valves 14, 22, 23, and 24, while working reference gas is introduced through the critical orifice at valve 24. From the intermediate volume, samples are expanded into the multipass cell for measurement, and evacuated by vacuum pumps after measurement, as described in Sect. 2.1. Inset: spectral windows covered by the two quantum cascade lasers, showing the absorbance features used to quantify $^{14}N^{15}N^{16}O$, $^{15}N^{14}N^{16}O$, and $^{15}N^{15}N^{16}O$ using QCL1 and $^{14}N^{14}N^{17}O$, $^{14}N^{14}N^{18}O$, $^{14}N^{15}N^{18}O$, and $^{15}N^{14}N^{18}O$ using QCL2.

by stainless-steel tubing, and is evacuated stepwise by a screw (PDV500, Ebara, Japan) and a turbomolecular pump (HiCube Eco 80, Pfeiffer Vacuum, Germany). It allows defined amounts of N_2, 8 % N_2O-in-N_2 working gas, and samples to be delivered to the intermediate gas volume (Fig. 1), from which they can then be expanded into the multipass cell. Gas flows into the inlet system are controlled by critical orifices, as shown on Fig. 1, including two options for sample introduction (30, 50 µm). The operation of the spectrometer and inlet system are coordinated by custom scripts within the spectrometer control software (TDLWintel, Aerodyne). Samples are typically delivered to the spectrometer in 10 mL stainless steel cylinders (Arbor Fluidtec-Swagelok, Switzerland) containing between 30 µmol and 2 mmol of pure N_2O.

A sample-measurement cycle consists of three sample injections, each bracketed by injections of 8 % N_2O-in-N_2 working reference gas (PanGas, Switzerland). For each working reference gas aliquot, the intermediate volume is filled to the target pressure of 27 hPa with 8 % N_2O-in-N_2, while for each sample gas aliquot, pure N_2O is introduced into the intermediate volume first (2.2 hPa) and then topped up to a total pressure of 27.0 hPa with N_2 (6.0 grade). On expansion into the multipass cell, sample and reference gas aliquots yield a pressure of 4.8 hPa. Spectral data are collected for two minutes for each injection, during which time the next sample or working reference gas aliquot is prepared in the inlet system. At the end of each measurement phase the cell is evacuated to < 0.02 hPa and the next gas aliquot is introduced within one minute.

Absorption spectra are recorded at 1 s temporal resolution and concentrations of individual isotopologues are quantified in real time by TDLWintel (Aerodyne Research Inc.). Ratios R^i_{raw} of individual isotopologues i to the main isotopic species $^{14}N^{14}N^{16}O$ are calculated for both sample and working reference gases. Then, delta values (δ^i) are calculated for each sample gas aliquot, normalized against the preceding and following working reference gas measurements, according to Eq. (1):

$$\delta^i = \left(R^i_{\mathrm{raw,\,sample}} / R^i_{\mathrm{raw\ work\ ref}}\right) - 1 + \delta^i_{\mathrm{work\ ref}} \quad (1)$$

Finally, δ^i are corrected for concentration dependency effects by normalizing to the ratio of $^{14}N^{14}N^{16}O$ between sample and working reference. For the singly substituted isotopologues $^{14}N^{15}N^{16}O$, $^{15}N^{14}N^{16}O$, $^{14}N^{14}N^{18}O$, and $^{14}N^{14}N^{17}O$, delta values $\delta^{15}N^{\alpha}$, $\delta^{15}N^{\beta}$, $\delta^{18}O$, and $\delta^{17}O$ are reported on the international isotope ratio scales, Air-N_2 and VSMOW, respectively. The values for the working reference gas were assigned by measurement against the refer-

ence material RM1A (Mohn et al., 2022). For the clumped isotopologues $^{14}N^{15}N^{18}O$, $^{15}N^{14}N^{18}O$, and $^{15}N^{15}N^{16}O$, the parameter Δi describes the abundance of isotopologue i relative to a stochastic reference frame (Eiler, 2007; Magyar et al., 2016). As an intermediate parameter, we also define $\Delta^* i$, the clumped isotopic abundance calculated as if the working gas has a composition Δi of 0 ‰ for all isotopologues, and so then the measured δ^i of these isotopologues against the working reference gas can be converted to values of $\Delta^*{}^{14}N^{15}N^{18}O$, $\Delta^*{}^{15}N^{14}N^{18}O$, and $\Delta^*{}^{15}N^{15}N^{16}O$ by accounting for the Δi of the working gas.

2.2 Preparation of isotopically-labelled gases

By mixing highly isotopically-enriched $^{14}N^{15}N^{18}O$, $^{15}N^{14}N^{18}O$, $^{15}N^{15}N^{16}O$, and $^{14}N^{14}N^{18}O$, prepared previously by thermal decomposition of labelled ammonium nitrate (Kantnerová et al., 2020a; Mohn et al., 2022), with natural-abundance N_2O, we created reservoirs of N_2O "isotopically-spiked" to ~ 500 ‰ in each of these isotopologues. Briefly, a defined volume of the isotopologue of interest was injected into an evacuated 2 L high-pressure cylinder using a Vici multi-position valve (Vici Valco, USA) equipped with a sample loop. After flushing the loop with natural abundance N_2O the cylinder was topped off to ~ 32 bar. The total amount of added N_2O was determined gravimetrically (PBK987-B60, Mettler-Toledo, Switzerland). The prepared gases were used for the experiments described in the following sections.

2.3 Equilibration of N_2O over γ-Al_2O_3

For equilibration of N_2O over γ-Al_2O_3, we used a vertical tube furnace (Vevor, China) with a custom glass reaction vessel, which was attached to a vacuum line for sample introduction and collection and evacuated by an oil-free rotary (NeoDry 7E, Kashiyama, Japan) and a turbomolecular pump (HiCube Eco 80, Pfeiffer). This system, depicted in Fig. S1 in the Supplement was developed from the equilibrium furnace described in Zhang et al. (2025). The pressure in the vacuum line was monitored with a pair of gauges for pressures below 1 mbar (PKR361, Pfeiffer) and between 0 and 4 bar (Leo 1, Keller Pressure, Switzerland). The bottom of the glass reaction vessel was loaded with 1.0 g of γ-Al_2O_3, provided as cylindrical pellets 1.8" (3.16 mm) in diameter and $\sim$ 2–7 mm long (Aluminum oxide, γ-phase, catalyst support, high surface area; ThermoFisher, Germany). The pellets extended to a height of $\sim$ 1 cm in the vessel. The same γ-$Al_2O_3$was used for all experiments without replacement. The temperature of the reactor was monitored with a K-type thermocouple placed at its very bottom, alongside the catalyst pellets, and logged (Hobo, Onset Computer, USA). The uncertainty in equilibration temperature was estimated as ± 2 K, dominated by a temperature gradient in the reaction vessel (1.3 K cm^{-1}) and the temporal variation of the furnace temperature (± 1.0 K).

In a first series of experiments, we explored the role of temperature in γ-Al_2O_3 activation by sequentially pre-heating the catalyst at increasing temperatures between 338 and 551 °C. In each experiment, the catalyst was heated for $\sim$ 1 h while the reaction vessel was evacuated with the turbomolecular pump. The pressure over the catalyst typically rose to between 0.01 and 0.1 mbar during this pre-heating phase, before returning to < 0.01 mbar. Then, the equilibration vessel was restored to 200 °C, and once the temperature stabilized, 1.2 mmol of $^{14}N^{15}N^{18}O$- or $^{15}N^{14}N^{18}O$-spiked N_2O ("458-spike", "548-spike") was introduced. After a duration of at least 20 h, N_2O was cryogenically trapped out of the reaction vessel, expanded in a known volume to estimate the N_2O recovery, stored in a 10 mL stainless steel cylinder for storage until analysis, and then analyzed by QCLAS as described in Sect. 2.1.

After the temperature threshold for catalyst activation was established, further experiments, with incubation periods between 6 and 162 h, were conducted to establish the equilibrium nature and evaluate the kinetics of the reactions of N_2O isotopologues over γ-Al_2O_3. For these experiments, the catalyst was periodically re-activated by heating at 550 °C for > 1 h. Once activated, the catalyst was kept under vacuum ($\sim 10^{-6}$ mbar) and reactivation was not required for ≥ 1 month. For each equilibration experiment, the temperature of the reaction vessel was set between 153 and 220 °C, and either 0.3 or 1.2 mmol of N_2O of various isotopic compositions was introduced. At the end of each experiment, N_2O was cryogenically collected and analyzed as described in the Sect. 2.1.

2.4 Thermal decomposition of N_2O over γ-Al_2O_3

To determine the isotopic fractionation effects during thermal decomposition of N_2O over γ-Al_2O_3, a series of experiments was conducted in which 500 µmol of isotopically-labelled or natural-abundance N_2O was exposed to the catalyst at 498 °C. After reaction durations of 15–64 min, residual N_2O was extracted cryogenically and decomposition products, likely N_2, O_2, and NO (Lewis and Hinshelwood, 1938), were removed under vacuum. The collected N_2O was stored in a 10 mL stainless steel cylinder for subsequent isotope analysis. The kinetic isotope effects of thermal decomposition ($^{15}\varepsilon$, $^{18}\varepsilon$, and εSP) were quantified using a closed-system Rayleigh model and the expression $\delta = \delta_0 - \varepsilon \ln[N_2O]/[N_2O]_0$, where δ_0 is the starting isotopic composition.

3 Results and Discussion

3.1 Spectrometer performance

Optimal averaging times and calibration intervals for the spectrometer were evaluated by analyzing 8 % N_2O-in-N_2 working reference gas at the typical cell operating pressure of 4.8 hPa and using the Allan–Werle variance technique (Werle et al., 1993) (Fig. 2). We achieved Allan deviation minima of < 0.2 ‰ for all isotopologue ratios in less than 100 s, but observed impaired performance for integration times of more than 500 s, due to drift effects. This precision is adequate to resolve differences observed to date among natural or experimental materials (Kantnerová et al., 2020b, 2022; Magyar, 2017; Magyar et al., 2016) or predicted in literature (Schmidt and Johnson, 2015; Wang et al., 2004; Yeung, 2016), and matches or exceeds previous approaches (Kantnerová et al., 2020a; Magyar et al., 2016). To achieve the same precision for samples, rapid sample – reference switching is essential, so we established and optimized a measurement scheme to analyze one "reference–sample–reference" set in 480 s and triplicate sample analyses in less than 20 min. Since all samples are measured against the same internal working reference gas, results can be compared for samples measured in different analytical sessions. In addition, we find that the magnitude and even sign of concentration dependence correction associated with each isotopologue can vary over time. Such variation has been observed in another recent study measuring ^{17}O in CO_2 by laser spectroscopy (Ellis et al., 2025) and supports our approach of determining a specific concentration correction factor for each sample. To test its performance, we introduced repeated injections of working reference gas into the spectrometer over the course of $\sim$ 15 min and processed the data as if half of the pulses were a sample; the standard error for three "sample" pulses, each bracketed by two "reference" pulses, ranged from 0.09 ‰ to 0.18 ‰ for all isotopologue ratios (Fig. S2).

3.2 Catalyst activation

We tested the effect of different pre-treatment conditions, including temperatures, heating sources and duration, and evacuation on the activity of γ-Al_2O_3 for catalyzing isotope exchange reactions in N_2O. Preliminary experiments showed that heating γ-Al_2O_3 with a natural gas torch under vacuum, as described by Magyar et al. (2016) and Kantnerová et al. (2020a), resulted in inconsistent results. Therefore, using the on-line furnace described in Sect. 2.3 we systematically tested the influence of activation temperature on isotope exchange. We evaluated activation by heating $^{14}N^{15}N^{18}O$-spiked N_2O, with a $\Delta^{*14}N^{15}N^{18}O$ of 512 ‰, under consistent conditions and found a sharp activation threshold between 467 and 515 °C (Fig. 3). Using a logistic fit to these data we estimate the midpoint temperature of the activation path as 490 ± 4 °C (1 SE). Catalyst activation at temperatures below this threshold led to only subtle changes in $\Delta^{*14}N^{15}N^{18}O$, while catalyst activated at 515 °C and higher uniformly showed a drop of > 400 ‰ towards expected equilibrium values. These results are consistent with the choice of temperatures between 550 and 567 °C to activate γ-Al_2O_3 for catalysis of exchange among methane clumped isotopologues and between CH_4, H_2, and other hydrocarbons, which in turn followed from the temperature required to convert boehmite, γ-AlO(OH), to γ-Al_2O_3 (Eldridge et al., 2019; Robertson et al., 1975; Wang et al., 2020a). Although it has been shown that γ-Al_2O_3 does not serve as a catalyst for methane isotope equilibration in the absence of thermal activation (Turner et al., 2021), the lower threshold of activation has not been explored thoroughly. In a subset of experiments, we also activated γ-Al_2O_3 at 550 °C in the presence of O_2, but did not observe quantifiable effects on catalytic activity; these experiments were again motivated by work with methane and hydrocarbons in which such an oxygen activation step is included to enhance catalytic activity (Eldridge et al., 2019, 2023; Robertson et al., 1975; Turner et al., 2021). Based on the outcome of these experiments, we chose 550 °C and a minimum of 1 h as standard catalyst activation conditions for subsequent experiments.

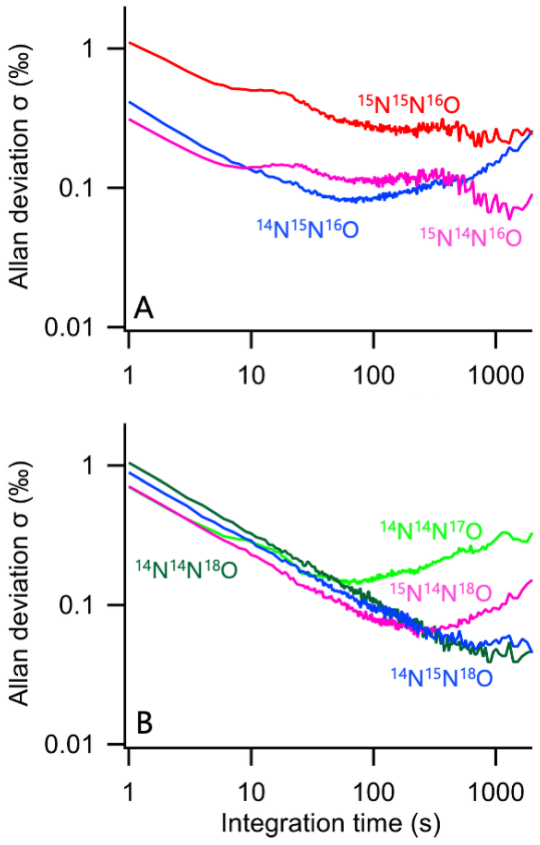

Figure 2. Allan–Werle deviation plots for isotopologues measured by QCL1 **(A)** and QCL2 **(B)**.

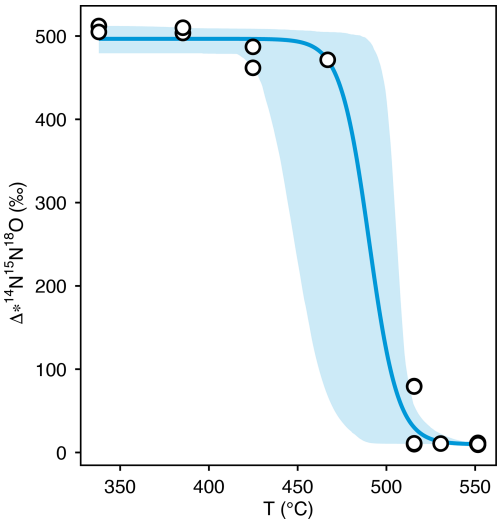

Figure 3. Threshold temperature for activation of γ-Al_2O_3 for equilibration of N_2O isotopologues. Data points show the abundance of $^{14}N^{15}N^{18}O$, as described by the parameter $\Delta^{*14}N^{15}N^{18}O$, for $^{14}N^{15}N^{18}O$-spiked N_2O heated over γ-Al_2O_3 after its activation at the denoted temperature. The blue curve and band represent a logistic fit and associated 95 % confidence interval, yielding estimates of 497 ± 9 ‰, 10 ± 7 ‰, 490 ± 4 °C, and 0.12 ± 0.02 for the isotopic composition before and after activation, the threshold temperature, and the exponential factor k describing the fit, respectively. Error bars (1 SE for three replicate measurements of a given sample gas) are smaller than the marker size.

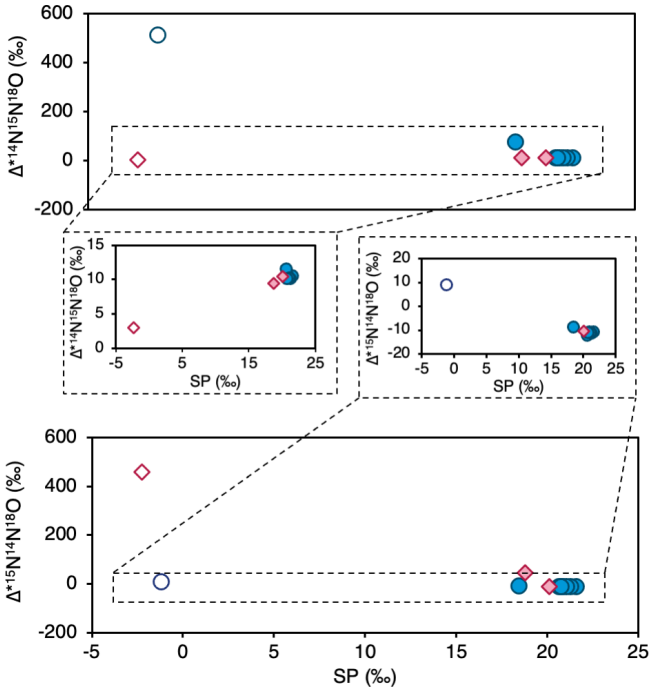

Figure 4. Convergence of isotopic parameters on a common composition. Starting materials (hollow symbols) that bracket the expected equilibrium composition in $\Delta^{*14}N^{15}N^{18}O$, $\Delta^{*15}N^{14}N^{18}O$, and SP were heated over activated γ-Al_2O_3 and are observed to converge on a narrow range in all parameters (filled symbols). Zoomed plots (dashed insets) show that this convergence is observed even over finer scales in $\Delta^{*14}N^{15}N^{18}O$ and $\Delta^{*15}N^{14}N^{18}O$ for the complementary isotopologues to the ones specifically spiked into the starting materials used.

3.3 Establishing the equilibrium nature of the reaction of N_2O over γ-Al_2O_3

To establish that the reactions undergone by N_2O isotopologues in the presence of γ-Al_2O_3 are of an equilibrium nature, we relied on three lines of evidence: (1) convergence on a common isotopic composition from distinctly different starting materials; (2) time-invariance of isotopic composition for extended time intervals after convergence; and (3) matching theoretical temperature dependence predictions. The first two criteria, the principles of convergence and time-invariance, have a strong basis in isotope geochemistry to identify equilibrium reactions in geochemical or petrological settings (O'Neil, 1986). The materials described in Sect. 2.2, with elevated values of $\Delta^{*14}N^{15}N^{18}O$ and $\Delta^{*15}N^{14}N^{18}O$, were exposed to the activated catalyst at 200 °C for durations between 6 and 117 h. We found that after one day these materials had converged on narrow ranges in $\Delta^{*14}N^{15}N^{18}O$ and $\Delta^{*15}N^{14}N^{18}O$ (Fig. 4), and that rapid progress towards that range was already achieved after 6 h (Fig. 5). For $\Delta^{*14}N^{15}N^{18}O$, starting materials at 512 ‰, 3.0 ‰, and −0.3 ‰ converged to 10.32 ± 0.60 ‰, apart from one experiment, which displayed a residual $\Delta^{*14}N^{15}N^{18}O$ of 79.7 ‰ after 24 h. This outlier, for the first sample measured after γ-Al_2O_3 activation at the lower temperature threshold (515 °C), suggests as-yet uncharacterized complexity to the activation of γ-Al_2O_3, and the need to verify results by repetitive equilibration experiments. Likewise, for $\Delta^{*15}N^{14}N^{18}O$, a value of -11.07 ± 0.55 ‰ was converged upon from starting materials at 458.6 ‰, 9.1 ‰, and 0.0 ‰. At the same time, for all equilibration experiments on N_2O with enhanced $\Delta^{*14}N^{15}N^{18}O$ and $\Delta^{*15}N^{14}N^{18}O$, SP values increased from ~ -2 ‰ to 0 ‰ in the starting materials to 20.9 ± 0.4 ‰ after 24 h (Fig. 5). This robust convergence on a putative equilibrium isotopic composition is our first indication of equilibrium reactions at work, for the three parameters SP, $\Delta^{*14}N^{15}N^{18}O$, and $\Delta^{*15}N^{14}N^{18}O$.

Complementary to convergence is time-invariance of isotopic composition after equilibrium has been reached, as long as thermodynamic conditions remain constant. This was confirmed by consistency of SP values at 20.9 ± 0.4 ‰, even when heating for durations of up to one week (162 h) (Fig. 5). Likewise, in all cases where the catalyst was activated at 550 °C, and in all but one case for an activation between 515 and 550 °C, the values of $\Delta^{*14}N^{15}N^{18}O$ and $\Delta^{*15}N^{14}N^{18}O$ achieved at 24 h were the same as those seen out to one week (162 h) (Fig. 5). In contrast, any kinetic effect associated with N_2O decomposition or rearrangement is expected to lead to

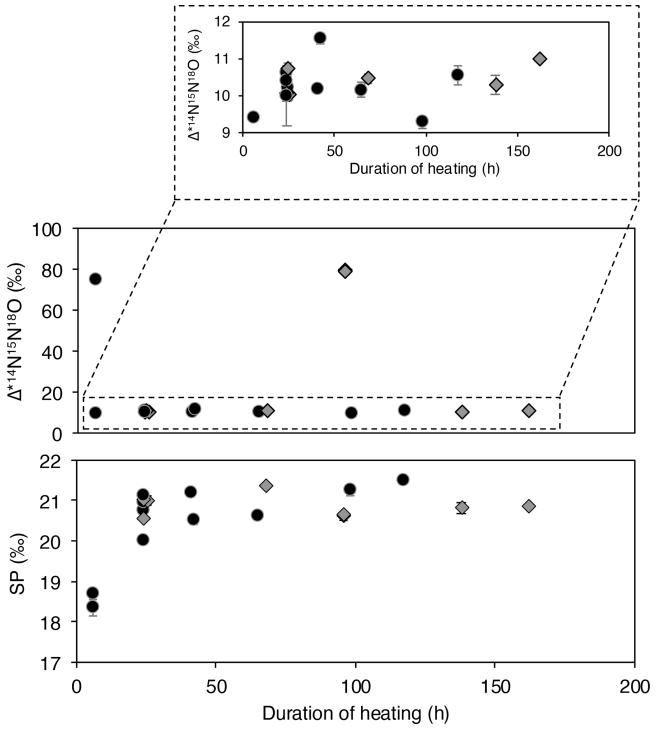

Figure 5. Time-invariance of $\Delta^{*14}N^{15}N^{18}O$ and SP for extended durations of heating at 200 °C. For all samples heated over γ-Al_2O_3, which wasactivated at 550 °C (black circles), and most samples with activation between 515 and 550 °C (gray diamonds), values of these parameters remain at the value they reach in 24 h for durations up to one week. Error bars represent 1 standard error for replicate measurements of a given sample; when not seen, error bars are smaller than the marker size. The inset shows a zoomed-in view of variation in $\Delta^{*14}N^{15}N^{18}O$ for samples close to the equilibrated value.

continuous evolution in isotopic composition for as long as concentration continues to change. A more specific comparison of isotopic evolution under kinetic and equilibrium conditions is discussed in Sect. 3.4.

The third confirmation that equilibration has been reached is the agreement with theoretical predictions of differences in $\Delta^{*14}N^{15}N^{18}O$, $\Delta^{*15}N^{14}N^{18}O$, and SP for different equilibration temperatures. Based on the Urey–Bigeleisen–Mayer quantum statistical mechanical framework using anharmonic potential energy surfaces (Bigeleisen and Friedman, 1950; Bigeleisen and Mayer, 1947; Cao and Liu, 2012; Urey, 1947; Wang et al., 2004), and validated by a Feynman path-integral approach (Webb and Miller, 2014), we have robust estimates for $\Delta^{14}N^{15}N^{18}O$, $\Delta^{15}N^{14}N^{18}O$, and SP at equilibrium (Fig. 6). We introduced N_2O over γ-Al_2O_3 and held it at temperatures of 154, 178, 191 and 218 °C. We compare the results to the experiments conducted for >24 h at 200 °C, discussed in the preceding sections. This temperature range was chosen based on the slow kinetics seen between 25 and 100 °C and enhanced decomposition at temperatures above 200 °C observed previously (Kantnerová et al., 2020a; Magyar et al., 2016). For SP, theoretical predictions indicate differences of 5.23 ± 0.24 ‰ for N_2O equilibrated at 154 °C relative to 218 °C, which agrees within analytical uncertainties with the observed span of 4.92 ± 0.17 ‰ (Fig. 6). Changes seen for the clumped parameters $\Delta^{*14}N^{15}N^{18}O$ and $\Delta^{*15}N^{14}N^{18}O$ for N_2O equilibrated between 154 and 218 °C also match theoretical predictions, but with more scatter around the expected values (Fig. 6). For instance, for $\Delta^{*15}N^{14}N^{18}O$, experimental results for the maximum (218 °C) and minimum (154 °C) temperatures show an offset of -2.5 ± 0.3 ‰, matching the expected value of -2.7 ± 0.12 ‰, but deviations from theoretical predictions are seen for measurements at 178 and 191 °C. It is not clear whether these deviations arise from the larger analytical uncertainty of clumped isotope measurements relative to a smaller predicted range in the parameters $\Delta^{*14}N^{15}N^{18}O$ and $\Delta^{*15}N^{14}N^{18}O$, or incomplete equilibration of these doubly substituted isotopologues in the time allotted, especially at lower temperatures. Finally, while the variation in SP, $\Delta^{*14}N^{15}N^{18}O$, and $\Delta^{*15}N^{14}N^{18}O$ between 154 and 218 °C matches equilibrium temperature dependencies well, a systematic offset is observed between the theoretical predictions and observed values for all three parameters. The interpretation and application of this offset is discussed further for the clumped isotopologues in Sect. 3.6, and for SP in Sect. 3.7.

The behavior of N_2O heated at 218 °C requires further discussion. When the amount of N_2O typical for other experiments, ~ 1.2 mmol, was introduced over γ-Al_2O_3 at this temperature, we did not see convergence in SP, $\Delta^{*14}N^{15}N^{18}O$, or $\Delta^{*15}N^{14}N^{18}O$ (Fig. S3). We posit that above 200 °C, reactions associated with thermal decomposition may start to outpace isotope exchange reactions and impart a kinetic isotope effect. However, when only 0.3 mmol of N_2O was introduced to the catalyst, we found that it converged on values of SP, $\Delta^{*14}N^{15}N^{18}O$, and $\Delta^{*15}N^{14}N^{18}O$ consistent with outcomes at other temperatures, even with relatively poor yields of 50 %–70 %. Whether this empirical result depends on variations in the relative kinetics of exchange to decomposition at different catalyst-to-N_2O ratios, or differences of the pressure dependencies of these two reactions, remains to be explored further. Subsequently, a 300 µmol N_2O sample was reacted over γ-Al_2O_3 at 200 °C, where its composition was found to be indistinguishable from 1200 µmol samples; its results are reported among those already discussed.

3.4 Thermal decomposition can be distinguished from equilibration

We posited in the preceding section that through the expression of a kinetic isotope effect, thermal decomposition would be expected to lead to continuous evolution in the isotopic composition of all isotopologue ratios in

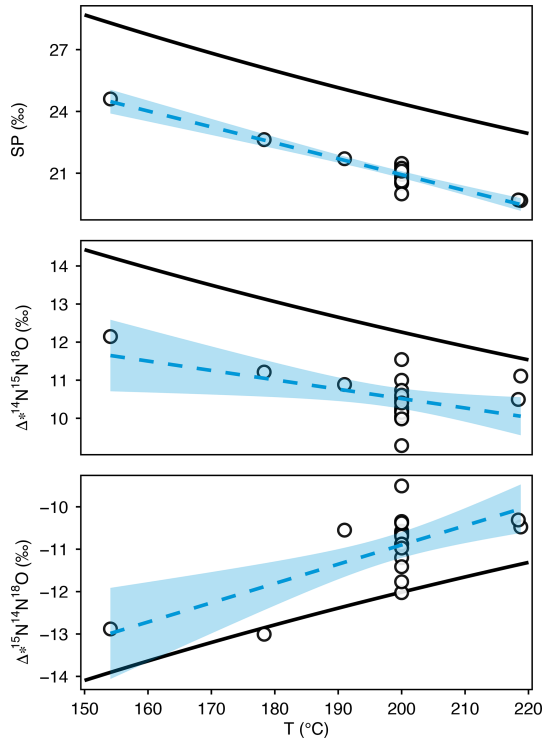

Figure 6. Achievement of expected temperature dependence for SP, $\Delta^{*14}N^{15}N^{18}O$, and $\Delta^{*15}N^{14}N^{18}O$. Black circles show measured data, while the black curve shows the predicted temperature variation. Experiments at 218 °C were performed with 300 µmol N_2O, as was one experiment at 200 °C (see Sect. 3.3). All other experiments were performed with 1200 µmol N_2O. All three parameters follow the expected temperature dependence, as indicated by linear regressions and associated 95 % confidence intervals (blue curve and shading), between 154 and 218 °C. All parameters also show an offset from the theoretical predictions, which is discussed in Sect. 3.6 and 3.7.

the residual fraction as N_2O is destroyed, and that thereby it can readily be distinguishable from equilibrium isotope effects. To provide an explicit comparison, we evaluated the isotopic evolution of $\Delta^{*14}N^{15}N^{18}O$-spiked and natural-abundance N_2O subjected to heating at 498 °C in the presence of γ-Al_2O_3 (Fig. 7). In both experiments, nearly half of the supplied N_2O was destroyed within 15 min, reaching about 80 % after one hour. Nitrogen isotope effects $^{15}\varepsilon$ of 3 ‰–5 ‰ and oxygen isotope effects $^{18}\varepsilon$ of 5 ‰–9 ‰ were observed, reflecting an increased durability of heavy isotopologues relative to $^{14}N^{14}N^{16}O$ (Bigeleisen, 1949), with higher values for $\Delta^{*14}N^{15}N^{18}O$-spiked N_2O. Both $^{15}\varepsilon$ and $^{18}\varepsilon$ are of smaller magnitude than the isotope effects reported for homogeneous decomposition of N_2O in quartz-glass tubes at 1000 °C (Ogawa and Yoshida, 2004). Surprisingly, $^{14}N^{15}N^{16}O$ and $^{15}N^{14}N^{16}O$ are decomposed at similar rates with a slight preference for destruction of $^{14}N^{15}N^{16}O$ (Fig. 8), resulting in an εSP of ~ -1 ‰ (Fig. S4). In contrast, previous observations of thermal decomposition and of the destruction of N_2O by photolysis or by bacterial reduction all found distinct enrichment in SP, rationalized by a ^{15}N–^{16}O bond stronger than the ^{14}N–^{16}O alternative (Kantnerová et al., 2020b; Ogawa and Yoshida, 2004; Ostrom et al., 2007). The final element of differentiation between kinetic and equilibrium effects comes from the behavior of $\Delta^{*14}N^{15}N^{18}O$ and $\Delta^{*15}N^{14}N^{18}O$. With increasing decomposition, $\Delta^{*14}N^{15}N^{18}O$ decreased in both natural-abundance and spiked N_2O, while $\Delta^{*15}N^{14}N^{18}O$ increased for spiked N_2O and remained constant for natural abundance N_2O. For neither starting N_2O do $\Delta^{*14}N^{15}N^{18}O$ and $\Delta^{*15}N^{14}N^{18}O$ approach the values of 5.7 ‰ and −5.6 ‰ predicted for equilibrium at 498 °C (Fig. 7). Together these pieces of evidence lead us to conclude that some amount of rearrangement among isotopologues accompanies decomposition.

With these results in mind, we revisit the equilibration experiments described in the preceding section. In the ideal situation where only an equilibrium isotope effect is acting on these N_2O samples over γ-Al_2O_3, the amount of N_2O would not change. This was clearly observed for lower equilibration temperatures (154, 178, 191 °C) with yields of 90 %–95 %, while experiments at intermediate (200 °C) and higher temperatures (218 °C) for comparable experimental periods showed reduced yields of 70 %–90 % and 50 %–70 %, respectively. To further evaluate any imprint of kinetic isotope effects associated with this extent of decomposition, we consider the evolution of the bulk isotope composition over the course of equilibration experiments. We find that indeed the subtle variation seen in $\delta^{18}O$ and $\delta^{15}N$ across all equilibrium experiments matches the expression of the kinetic isotope effects determined here, but that SP and the clumped parameters $\Delta^{*14}N^{15}N^{18}O$ and $\Delta^{*15}N^{14}N^{18}O$ do not appear to be controlled by these kinetic isotope effects (Fig. 9). Nevertheless, we cannot exclude the possibility that some of the variation seen in repeated measurements at 200 °C comes from variable expression of kinetic isotope effects. Indeed, a decomposition fraction of 30 % could drive changes in SP, $\Delta^{*14}N^{15}N^{18}O$, and $\Delta^{*15}N^{14}N^{18}O$ of −0.36 ‰, −1.59 ‰, and 1.42 ‰, respectively, and so could contribute to the variability seen in repeated equilibrium experiments (Sect. 3.6 and 3.7, Table S1 in the Supplement). Therefore, an important element of any subsequent application of this work will be to choose experimental conditions that minimize decomposition and maximize yield, while still achieving complete exchange.

3.5 The case of $^{15}N^{15}N^{16}O$

In a preliminary series of experiments, N_2O spiked in $\Delta^{*15}N^{15}N^{16}O$ was also heated over γ-Al_2O_3. Here we found that even after 94 h at 200 °C the value of $\Delta^{*15}N^{15}N^{16}O$ remained elevated at 558 ‰. Therefore, we conclude that the catalyst γ-Al_2O_3 only activates the N–O bond in N_2O, and not the N–N bond, and accordingly facilitates equilibrium isotope reactions among position-specific and ^{18}O-bearing

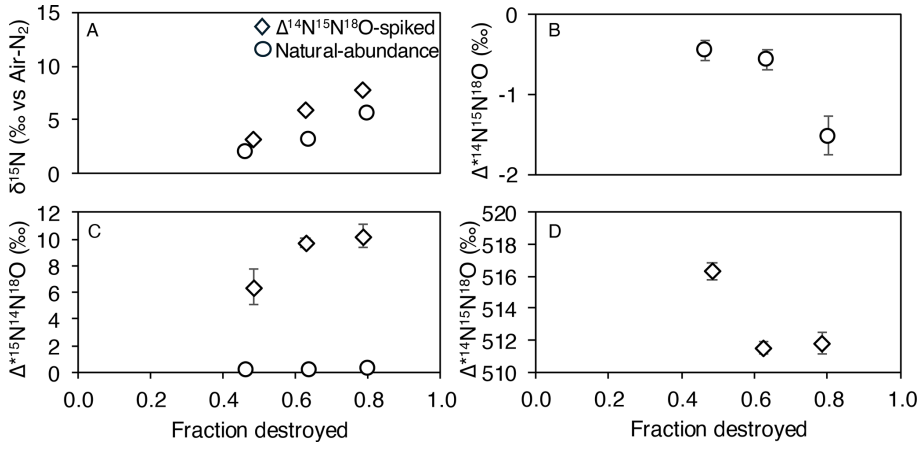

Figure 7. Evolution of $\delta^{15}N$, $\Delta^{*14}N^{15}N^{18}O$, and $\Delta^{*15}N^{14}N^{18}O$ for N_2O subjected to thermal decomposition at 498 °C. Panels **(A)** and **(C)** show the outcomes for both $\Delta^{*14}N^{15}N^{18}O$-spiked (diamonds) and natural-abundance (circles) starting materials for the parameters $\delta^{15}N$ and $\Delta^{*15}N^{14}N^{18}O$, while panels **(B)** and **(D)** show the offset variation in $\Delta^{*14}N^{15}N^{18}O$ seen for starting materials distinctly different in this parameter. Error bars represent 1 standard error for replicate measurements of a given sample.

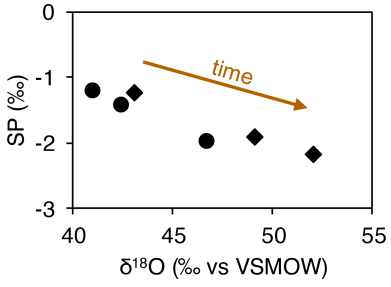

Figure 8. Coevolution of SP and $\delta^{18}O$ over the course of thermal decomposition. Diamonds represent $\Delta^{*14}N^{15}N^{18}O$-spiked starting material, while circles represent natural abundance N_2O.

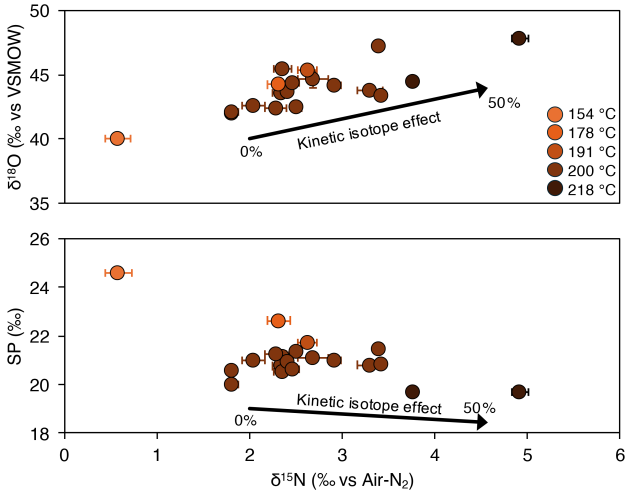

Figure 9. $\delta^{18}O$ and SP versus $\delta^{15}N$ for N_2O equilibrated over γ-Al_2O_3 at 154–214 °C (denoted by colors). The black arrows indicate the measured kinetic isotope effect of thermal decomposition at 498 °C (50 % destruction) shown for comparison. Error bars show 1 SE for three replicate measurements of a sample; when absent standard errors are smaller than the datapoints.

isotopologues, but not those involving $^{15}N^{15}N^{16}O$. To find alternative catalysts or conditions that activate $^{15}N^{15}N^{16}O$ remains a challenge for future work. In the meantime, it is impossible to establish an absolute reference frame for $\Delta^{15}N^{15}N^{16}O$ and so we will continue to report results on a relative basis as $\Delta^{*15}N^{15}N^{16}O$; such an approach has also been proposed and applied for ethane and other compounds recalcitrant to equilibration (Clog et al., 2018; Gilbert, 2021).

3.6 Establishing absolute reference frames for $\Delta^{14}N^{15}N^{18}O$ and $\Delta^{15}N^{14}N^{18}O$

Having found that the abundances of the isotopologues $^{14}N^{15}N^{18}O$ and $^{15}N^{14}N^{18}O$ can be brought to equilibrium isotopic distributions between 153 and 218 °C, we use this outcome to establish an absolute reference frame for future measurements of $\Delta^{14}N^{15}N^{18}O$ and $\Delta^{15}N^{14}N^{18}O$. Since 200 °C is the temperature where we evaluated the conditions of convergence and time-invariance and have the most robust replicated dataset, we use these measurements to determine the values of $\Delta^{14}N^{15}N^{18}O$ and $\Delta^{15}N^{14}N^{18}O$ of our working gas against a true stochastic distribution of rare isotopes among isotopologues. These values, reported in Table 1, can then be used to convert values of $\Delta^{*14}N^{15}N^{18}O$ and $\Delta^{*15}N^{14}N^{18}O$, as reported here or in future studies, to $\Delta^{14}N^{15}N^{18}O$ and $\Delta^{15}N^{14}N^{18}O$. Previous N_2O clumped isotope studies also sought to achieve such an absolute reference frame. Early mass spectrometric work was limited by the need to use measurements of $\Delta^{14}N^{15}N^{18}O$ in equilibrated samples to account for ion source scrambling in the genera-

Table 1. Comparison of theoretical predictions and measured values for SP, $\Delta^{14}N^{15}N^{18}O$, and $\Delta^{15}N^{14}N^{18}O$ for equilibration at 200 °C. Measured $\Delta^{14}N^{15}N^{18}O$, and $\Delta^{15}N^{14}N^{18}O$ values are reported relative to the working reference gas being 0 ‰, while measured SP values are reported using the value assigned by comparison with Science Tokyo (Mohn et al., 2022; Toyoda and Yoshida, 1999). Uncertainties represent 1 standard deviation for replicate experiments comprising independent equilibration and analysis.

	Prediction	Measured	Offset
SP	24.38 ‰	20.9 ± 0.4 ‰	−3.4 ‰
$\Delta^{14}N^{15}N^{18}O$	12.26 ‰	10.4 ± 0.5 ‰	−1.9 ‰
$\Delta^{15}N^{14}N^{18}O$	−12.01 ‰	-10.8 ± 0.6 ‰	1.2 ‰

tion of the $^{15}N^{18}O^+$ ion used to measure this isotopologue (Magyar et al., 2016), while first QCLAS studies lacked the full suite of convergence, time-invariance, and temperature dependency results used here to confirm the equilibrium nature of the reactions of N_2O isotopologues over γ-Al_2O_3 (Kantnerová et al., 2020a). By establishing this absolute reference scale and reporting future results on it, we enable their interpretation in the context of theoretical predictions or natural phenomena where the true distribution of isotopes among isotopologues is relevant, and we also facilitate comparisons among different labs and analytical approaches for measuring these parameters.

3.7 Implications for the absolute determination of SP

For N_2O equilibrated at 200 °C, we observed an offset of -3.43 ± 0.36 ‰ between predicted SP values and our repeated equilibration experiments (Table 1). This was not expected since SP is defined as the difference of two parameters, $\delta^{15}N^{\alpha}$ and $\delta^{15}N^{\beta}$, both connected through a chain of reference materials to the international Air-N_2 scale. Therefore, SP should reflect an absolute determination of the relationship of $^{14}N^{15}N^{16}O$ and $^{15}N^{14}N^{16}O$. The key point of connection is through the thermal decomposition of ammonium nitrate to N_2O, whereby $\delta^{15}N^{\alpha}$ and $\delta^{15}N^{\beta}$ values are assigned to N_2O by comparison to the precursor δ^{15}N-NO_3^- and δ^{15}N-NH_4^+,determined using established means and reference materials. This procedure has been repeated in a number of laboratories (Harris et al., 2014; Mohn et al., 2016, 2022; Toyoda and Yoshida, 1999; Westley et al., 2007). Currently, to maximize comparability among labs, the ammonium nitrate decomposition conducted at Tokyo Tech (Toyoda and Yoshida, 1999), now Science Tokyo, is commonly used as the basis for setting the $\delta^{15}N^{\alpha}$ and $\delta^{15}N^{\beta}$ for other laboratories and reference materials (Mohn et al., 2022; Ostrom et al., 2018). However, the decomposition of ammonium nitrate has been found to exhibit significant variation in assigned $\delta^{15}N^{\alpha}$ and $\delta^{15}N^{\beta}$ values, controlled by yield and isotopic fractionation (Mohn et al., 2016). Mohn et al. (2022) found an offset of −1.51 ‰ in SP between the outcome of ammonium nitrate decomposition according to current best practices and the reference frame based on Toyoda and Yoshida (1999). This deviation is in the same direction, although of smaller magnitude, as that estimated here from thermodynamic equilibrium; together these provide two lines of evidence to suggest an offset between the current international reference frame for $\delta^{15}N^{\alpha}$ and $\delta^{15}N^{\beta}$ and the true ratio of $^{14}N^{15}N^{16}O$ versus $^{15}N^{14}N^{16}O$. To follow up from this conclusion will require further equilibration experiments – best would be to subject international reference materials with well-characterized $\delta^{15}N$ and $\delta^{18}O$ to equilibration over γ-Al_2O_3 at optimal conditions for maximum yield. Thereby we can determine if the uncertainty in the results reported here is tied to the equilibration experiments themselves, including possible imprints of a kinetic isotope effect from thermal decomposition. This work can be coupled to further repeat measurements of equilibrated reference materials to evaluate any room for improvement in measurement or gas handling procedures. The outcome of such equilibrium experiments can also be compared to other approaches that provide an estimate of the absolute relationship between $^{14}N^{15}N^{16}O$ and $^{15}N^{14}N^{16}O$, whether novel spectroscopic methods (Griffith et al., 2009; Łapiński et al., 2001; Schlagin et al., 2025) or alternative experimental frameworks (Sadiek et al., 2025). If such experiments and measurements confirm the conclusions drawn here, the international N_2O isotopomer community will need to determine how to harmonize these latest results with the existing reference frame for $\delta^{15}N^{\alpha}$ and $\delta^{15}N^{\beta}$.

Finally, it is necessary to note that SP, defined as the difference in $\delta^{15}N$ between α and β nitrogen atoms, is only an approximation of the equilibrium constant for Reaction (R1), which is the ratio ${}^{15}R^{\alpha}/{}^{15}R^{\beta}$; for an equilibrated sample. As discussed in Magyar et al. (2016) and Sadiek et al. (2025), for some combinations of $\delta^{15}N^{\alpha}$ and $\delta^{15}N^{\beta}$ this difference becomes significant, but for the set of samples described in this study, and for many natural samples, SP is remarkably close as an approximation to the ratio ${}^{15}R^{\alpha}/{}^{15}R^{\beta}$. Here, the difference between this ratio and SP was between 0.001 ‰ and 0.3 ‰ across all samples. Therefore, we can quantitatively compare SP to predicted equilibrium constants.

4 Conclusion

This study provides a firm foundation for applying clumped isotopic analysis to investigate the reactions responsible for producing and destroying N_2O in natural systems. We present a comprehensive analytical toolkit for repeatably measuring seven isotopic parameters, including the clumped isotopologues $^{14}N^{15}N^{18}O$, $^{15}N^{14}N^{18}O$, and $^{15}N^{15}N^{16}O$, in N_2O samples as small as 20 µmol. Our measurements achieve a precision of 0.3 ‰ or better by triplicate analysis completed within 20 min using quantum cascade laser absorption spectroscopy.

Furthermore, we established reaction conditions for equilibration among N_2O isotopologues catalyzed by γ-Al_2O_3, thereby reliably producing N_2O with predicted SP, $\Delta^{14}N^{15}N^{18}O$, and $\Delta^{15}N^{14}N^{18}O$. The results of these equilibration experiments provide an absolute reference frame for the parameters $\Delta^{14}N^{15}N^{18}O$ and $\Delta^{15}N^{14}N^{18}O$. This reference frame allows robust evaluations of these parameters in natural samples, comparison to theoretical predications, and intercomparison of measurements among laboratories and across various analytical techniques.

For SP, the offset we observe between our results and theoretical predictions suggests that current measurements using established gas reference materials provide too low values. Given the high number of laboratories linked to the current realization of the scale, we recommend further work to establish a community-wide absolute reference frame. Over the past decade, great progress has been made towards reconciling and unifying the diverse analytical approaches used to determine the position-specific isotopic composition of N_2O. This progress has been driven both by methodological intercomparison studies (Harris et al., 2020; Mohn et al., 2014; Ostrom et al., 2018) and by improvement and harmonization of corrections for ion-source rearrangement in mass spectrometric analyses (Frame et al., 2014; Harris et al., 2014; Kelly et al., 2023). Collectively, these advances have helped the community to improve its internal consistency and enable intercomparability among diverse techniques and laboratories, thereby facilitating the comparison of laboratory and field measurements of N_2O. But to leverage the full potential of position-specific measurements to understand N_2O cycling in nature requires accurate knowledge of the absolute relationship between $\delta^{15}N^{\alpha}$ and $\delta^{15}N^{\beta}$. We propose that the equilibrium experiments described in this study provide the foundations for an improved understanding of position-specific ^{15}N incorporation in N_2O.

Appendix A: Isotopologue parameters and equilibrium constants

As described in Sect. 2.1, we describe the clumped isotopic composition of N_2O with Δi values. The full isotopic composition of N_2O is best accounted for as a system of equilibrium reactions (Wang et al., 2004), but individual Δi values are calculated from measured isotopologues. Practically, $\Delta^{14}N^{15}N^{18}O$ is calculated as

$$\Delta^{*14}N^{15}N^{18}O = \frac{R^{458}}{\left(\frac{1}{2}(R^{456}+R^{546})\right)R^{448}} - 1 \quad \text{(A1)}$$

relative to the working reference gas and then adjusted for its clumped isotope composition as described in Sect. 3.6. This equation for $\Delta^{14}N^{15}N^{18}O$ is closely related to the equilibrium reaction:

$$^{14}N^{15}N^{18}O + {}^{14}N^{14}N^{16}O \rightleftharpoons \frac{1}{2}{}^{14}N^{15}N^{16}O + \frac{1}{2}{}^{15}N^{14}N^{16}O + {}^{14}N^{14}N^{18}O. \quad \text{(AR1)}$$

Analogous expressions are used for $\Delta^{15}N^{14}N^{18}O$ and $\Delta^{15}N^{15}N^{16}O$.

For N_2O, it is also possible to define the ^{15}N site preference for ^{18}O containing isotopologues, SP^{18}. By analogy to SP, which is related to the equilibrium Reaction (R1), SP^{18} is related to the reaction

$$^{15}N^{14}N^{18}O \rightleftharpoons {}^{14}N^{15}N^{18}O \quad \text{(AR2)}$$

SP^{18} was defined by Kantnerová et al. (2020a) as

$$SP^{18} = \delta(^{14}N^{15}N^{18}O) - \delta(^{15}N^{14}N^{18}O) \quad \text{(A2)}$$

and by Magyar et al. (2016) as the ratio of abundances of the two isotopologues $^{14}N^{15}N^{18}O$ and $^{15}N^{14}N^{18}O$. As discussed in Sect. 3.6, these definitions will converge for most isotopic compositions. Since the individual clumped isotopologues $^{14}N^{15}N^{18}O$ and $^{15}N^{14}N^{18}O$ are already each directly related to an equilibrium reaction and can be expressed as a Δi value, we find it most insightful, as well as the best application of analytical capacities, to consider these on their own. Nevertheless, it is possible to calculate SP^{18} values from measured abundances of $^{14}N^{15}N^{18}O$ and $^{15}N^{14}N^{18}O$, and the parameter may prove to be useful in future studies of N_2O clumped isotope effects imparted by certain processes.

Code and data availability. The underlying data for this study are available at https://doi.org/10.5281/zenodo.21453238 (Magyar et al., 2026). Additional data are available from the corresponding author on request.

Supplement. The supplement related to this article is available online at https://doi.org/10.5194/amt-19-5267-2026-supplement.

Author contributions. Conceptualization: PMM, NK, IP, NZ, BT, JM. Methodology: PMM, NK, NZ, IP, SB, NC, BT, JM. Investigation: PMM. Resources: BT, JM, LE. Funding acquisition: JM, PMM. Supervision: JM, LE. Project administration: JM, PMM. Formal analysis: PMM. Data curation: PMM. Visualization: PMM. Writing – original draft: PMM. Writing – review and editing: all authors.

Competing interests. The contact author has declared that none of the authors has any competing interests.

Disclaimer. Publisher's note: Copernicus Publications remains neutral with regard to jurisdictional claims made in the text, pub-

lished maps, institutional affiliations, or any other geographical representation in this paper. The authors bear the ultimate responsibility for providing appropriate place names. Views expressed in the text are those of the authors and do not necessarily reflect the views of the publisher.

Acknowledgements. We thank Christoph Dyroff, Scott Herndon, and David Nelson from Aerodyne Research Inc. for assistance with spectrometer setup and optimization.

Financial support. This study was funded by the SNSF projects 7up (project number 200020_204907) and CITRA (project number CRSK-2_228699). This work is part of the project 24GRD03 MetHIR, which has received funding from the European Partnership on Metrology, co-financed from the European Union's Horizon Europe Research and Innovation Programme and by the Participating States. The Empa contribution has received funding from the Swiss State Secretariat for Education, Research and Innovation (SERI).

Review statement. This paper was edited by Mingjin Tang and reviewed by three anonymous referees.

References

Bajnai, D. and Hare, V. J.: Sensitivity of tunable infrared laser spectroscopic measurements of $\Delta^{17}O$ in CO_2 to analytical conditions, Atmos. Meas. Tech., 18, 7405–7419, https://doi.org/10.5194/amt-18-7405-2025, 2025.

Bernasconi, S. M., Müller, I. A., Bergmann, K. D., Breitenbach, S. F. M., Fernandez, A., Hodell, D. A., Jaggi, M., Meckler, A. N., Millan, I., and Ziegler, M.: Reducing Uncertainties in Carbonate Clumped Isotope Analysis Through Consistent Carbonate-Based Standardization, Geochem. Geophy. Geosy., 19, 2895–2914, https://doi.org/10.1029/2017GC007385, 2018.

Bigeleisen, J.: The Relative Reaction Velocities of Isotopic Molecules, J. Chem. Phys., 17, 675–678, https://doi.org/10.1063/1.1747368, 1949.

Bigeleisen, J. and Friedman, L.: The Infra-Red Spectra of $N^{15}N^{14}O^{16}$ and $N^{14}N^{15}O^{16}$. Some Thermodynamic Properties of the Isotopic N_2O Molecules, J. Chem. Phys., 18, 1656–1659, https://doi.org/10.1063/1.1747556, 1950.

Bigeleisen, J. and Mayer, M.: Calculation of equilibrium constants for isotopic exchange reactions, J. Chem. Phys., 15, 261–267, https://doi.org/10.1063/1.1746492, 1947.

Cancellieri, C., Gramatte, S., Politano, O., Lapeyre, L., Klimashin, F. F., Mackosz, K., Utke, I., Novotny, Z., Müller, A. M., Vockenhuber, C., Turlo, V., and Jeurgens, L. P. H.: Effect of hydrogen on the chemical state, stoichiometry and density of amorphous Al_2O_3 films grown by thermal atomic layer deposition, Surf. Interface Anal., 56, 293–304, https://doi.org/10.1002/sia.7282, 2024.

Cao, X. and Liu, Y.: Theoretical estimation of the equilibrium distribution of clumped isotopes in nature, Geochim. Cosmochim. Ac., 77, 292–303, https://doi.org/10.1016/j.gca.2011.11.021, 2012.

Clog, M., Lawson, M., Peterson, B., Ferreira, A. A., Neto, E. V. S., and Eiler, J. M.: A reconnaissance study of ^{13}C–^{13}C clumping in ethane from natural gas, Geochim. Cosmochim. Ac., 223, 229–244, https://doi.org/10.1016/j.gca.2017.12.004, 2018.

Eiler, J. M.: "Clumped-isotope" geochemistry – The study of naturally-occurring, multiply-substituted isotopologues, Earth Planet. Sc. Lett., 262, 309–327, https://doi.org/10.1016/j.epsl.2007.08.020, 2007.

Eiler, J. M. and Schauble, E. A.: $^{18}O^{13}C^{16}O$ in Earth's atmosphere, Geochim. Cosmochim. Ac., 68, 4767–4777, https://doi.org/10.1016/j.gca.2004.05.035, 2004.

Eldridge, D. L., Korol, R., Lloyd, M. K., Turner, A. C., Webb, M. A., Miller, T. F., and Stolper, D. A.: Comparison of Experimental vs. Theoretical Abundances of $^{13}CH_3D$ and $^{12}CH_2D_2$ for Isotopically Equilibrated Systems from 1 to 500 °C, ACS Earth Space Chem., 3, 1–18, https://doi.org/10.1021/acsearthspacechem.9b00244, 2019.

Eldridge, D. L., Turner, A. C., Bill, M., Conrad, M. E., and Stolper, D. A.: Experimental determinations of carbon and hydrogen isotope fractionations and methane clumped isotope compositions associated with ethane pyrolysis from 550 to 600 °C, Geochim. Cosmochim. Ac., 355, 235–265, https://doi.org/10.1016/j.gca.2023.06.006, 2023.

Ellis, N. M., Kafaie, K. R., Wehr, R., Nelson, D. D., Herndon, S. C., Yang, W., Dawson, T. E., and Stolper, D. A.: A Method for Rapid and Precise Triple Oxygen Isotope Measurements via High-Temperature Conversion to CO Followed by Nickel-Catalyzed CO to CO_2 Conversion and Laser Spectroscopy, Anal. Chem., 97, 27767–27778, https://doi.org/10.1021/acs.analchem.5c04851, 2025.

Frame, C. H., Deal, E., Nevison, C. D., and Casciotti, K. L.: N_2O production in the eastern South Atlantic: Analysis of N_2O stable isotopic and concentration data, Global Biogeochem. Cy., 28, 1262–1278, https://doi.org/10.1002/2013GB004790, 2014.

Gilbert, A.: The Organic Isotopologue Frontier, Annu. Rev. Earth Pl. Sc., 49, 435–464, https://doi.org/10.1146/annurev-earth-071420-053134, 2021.

Gonzalez, Y., Nelson, D. D., Shorter, J. H., McManus, J. B., Dyroff, C., Formolo, M., Wang, D. T., Western, C. M., and Ono, S.: Precise Measurements of $^{12}CH_2D_2$ by Tunable Infrared Laser Direct Absorption Spectroscopy, Anal. Chem., 91, 14967–14974, https://doi.org/10.1021/acs.analchem.9b03412, 2019.

Gramatte, S., Jeurgens, L. P. H., Politano, O., Simon Greminger, J. A., Baras, F., Xomalis, A., and Turlo, V.: Atomistic Simulations of the Crystalline-to-Amorphous Transformation of γ-Al_2O_3 Nanoparticles: Delicate Interplay between Lattice Distortions, Stresses, and Space Charges, Langmuir, 39, 6301–6315, https://doi.org/10.1021/acs.langmuir.2c03292, 2023.

Griffith, D. W. T., Parkes, S. D., Haverd, V., Paton-Walsh, C., and Wilson, S. R.: Absolute Calibration of the Intramolecular Site Preference of ^{15}N Fractionation in Tropospheric N_2O by FT-IR Spectroscopy, Anal. Chem., 81, 2227–2234, https://doi.org/10.1021/ac802371c, 2009.

Hare, V. J., Dyroff, C., Nelson, D. D., and Yarian, D. A.: High-Precision Triple Oxygen Isotope Analysis of Carbon Dioxide by Tunable Infrared Laser Absorp-

tion Spectroscopy, Anal. Chem., 94, 16023–16032, https://doi.org/10.1021/acs.analchem.2c03005, 2022.

Harris, E., Nelson, D. D., Olszewski, W., Zahniser, M., Potter, K. E., McManus, B. J., Whitehill, A., Prinn, R. G., and Ono, S.: Development of a Spectroscopic Technique for Continuous Online Monitoring of Oxygen and Site-Specific Nitrogen Isotopic Composition of Atmospheric Nitrous Oxide, Anal. Chem., 86, 1726–1734, https://doi.org/10.1021/ac403606u, 2014.

Harris, S. J., Liisberg, J., Xia, L., Wei, J., Zeyer, K., Yu, L., Barthel, M., Wolf, B., Kelly, B. F. J., Cendón, D. I., Blunier, T., Six, J., and Mohn, J.: N_2O isotopocule measurements using laser spectroscopy: analyzer characterization and intercomparison, Atmos. Meas. Tech., 13, 2797–2831, https://doi.org/10.5194/amt-13-2797-2020, 2020.

Kantnerová, K., Yu, L., Zindel, D., Zahniser, M. S., Nelson, D. D., Tuzson, B., Nakagawa, M., Toyoda, S., Yoshida, N., Emmenegger, L., Bernasconi, S. M., and Mohn, J.: First investigation and absolute calibration of clumped isotopes in N_2O by mid-infrared laser spectroscopy, Rapid Commun. Mass Sp., 34, https://doi.org/10.1002/rcm.8836, 2020a.

Kantnerová, K., Jespersen, M. F., Bernasconi, S. M., Emmenegger, L., Johnson, M. S., and Mohn, J.: Photolytic fractionation of seven singly and doubly substituted nitrous oxide isotopocules measured by quantum cascade laser absorption spectroscopy, Atmospheric Environ. X, 8, 100094, https://doi.org/10.1016/j.aeaoa.2020.100094, 2020b.

Kantnerová, K., Hattori, S., Toyoda, S., Yoshida, N., Emmenegger, L., Bernasconi, S. M., and Mohn, J.: Clumped isotope signatures of nitrous oxide formed by bacterial denitrification, Geochim. Cosmochim. Ac., 328, 120–129, https://doi.org/10.1016/j.gca.2022.05.006, 2022.

Kelly, C. L., Manning, C., Frey, C., Kaiser, J., Gluschankoff, N., and Casciotti, K. L.: pyisotopomer: A Python package for obtaining intramolecular isotope ratio differences from mass spectrometric analysis of nitrous oxide isotopocules, Rapid Commun. Mass Sp., 37, e9513, https://doi.org/10.1002/rcm.9513, 2023.

Łapiński, A., Spanget-Larsen, J., Waluk, J., and Radziszewski, J. G.: Vibrations of nitrous oxide: Matrix isolation Fourier transform infrared spectroscopy of twelve N_2O isotopomers, J. Chem. Phys., 115, 1757–1764, https://doi.org/10.1063/1.1383031, 2001.

Lewis, R. M. and Hinshelwood, C. N.: The thermal decomposition of nitrous oxide, P. Roy. Soc. Lond. A Mat., 168, 441–454, https://doi.org/10.1098/rspa.1938.0185, 1938.

Magyar, P. M.: Insights into pathways of nitrous oxide generation from novel isotopologue measurements, PhD thesis, California Institute of Technology, Pasadena, California, https://doi.org/10.7907/Z93776RJ, 2017.

Magyar, P. M., Orphan, V. J., and Eiler, J. M.: Measurement of rare isotopologues of nitrous oxide by high-resolution multi-collector mass spectrometry: Measurement of rare isotopologues of nitrous oxide, Rapid Commun. Mass Sp., 30, 1923–1940, https://doi.org/10.1002/rcm.7671, 2016.

Magyar, P. M., Kueter, N., Brunamonti, S., Zhang, N., Prokhorov, I., Chénier, N., Emmenegger, L., Tuzson, B., and Mohn, J.: Data for An absolute reference frame for nitrous oxide clumped and position-specific isotopes provided by thermal equilibration, Zenodo [data set], https://doi.org/10.5281/zenodo.21453238, 2026.

Mohn, J., Wolf, B., Toyoda, S., Lin, C.-T., Liang, M.-C., Brüggemann, N., Wissel, H., Steiker, A. E., Dyckmans, J., Szwec, L., Ostrom, N. E., Casciotti, K. L., Forbes, M., Giesemann, A., Well, R., Doucett, R. R., Yarnes, C. T., Ridley, A. R., Kaiser, J., and Yoshida, N.: Interlaboratory assessment of nitrous oxide isotopomer analysis by isotope ratio mass spectrometry and laser spectroscopy: current status and perspectives, Rapid Commun. Mass Sp., 28, 1995–2007, https://doi.org/10.1002/rcm.6982, 2014.

Mohn, J., Gutjahr, W., Toyoda, S., Harris, E., Ibraim, E., Geilmann, H., Schleppi, P., Kuhn, T., Lehmann, M. F., Decock, C., Werner, R. A., Yoshida, N., and Brand, W. A.: Reassessment of the NH_4NO_3 thermal decomposition technique for calibration of the N_2O isotopic composition, Rapid Commun. Mass Sp., 30, 2487–2496, https://doi.org/10.1002/rcm.7736, 2016.

Mohn, J., Biasi, C., Bodé, S., Boeckx, P., Brewer, P. J., Eggleston, S., Geilmann, H., Guillevic, M., Kaiser, J., Kantnerová, K., Moossen, H., Müller, J., Nakagawa, M., Pearce, R., von Rein, I., Steger, D., Toyoda, S., Wanek, W., Wexler, S. K., Yoshida, N., and Yu, L.: Isotopically characterised N_2O reference materials for use as community standards, Rapid Commun. Mass Sp., 36, e9296, https://doi.org/10.1002/rcm.9296, 2022.

Nataraj, A., Gianella, M., Prokhorov, I., Tuzson, B., Bertrand, M., Mohn, J., Faist, J., and Emmenegger, L.: Quantum cascade laser absorption spectrometer with a low temperature multipass cell for precision clumped CO_2 measurement, Opt. Express, 30, 4631, https://doi.org/10.1364/OE.447172, 2022.

Ogawa, M. and Yoshida, N.: Stable isotope fractionation of nitrous oxide during thermal decomposition and reduction processes, J. Geophys. Res.-Atmos., 109, 19301, https://doi.org/10.1029/2004JD004652, 2004.

O'Neil, J. R.: Theoretical and Experimental Aspects of Isotopic Fractionation, Rev. Mineral., 16, 1–40, 1986.

Ostrom, N. E. and Ostrom, P. H.: Mining the isotopic complexity of nitrous oxide: a review of challenges and opportunities, Biogeochemistry, 132, 359–372, https://doi.org/10.1007/s10533-017-0301-5, 2017.

Ostrom, N., Pitt, A., Sutka, R., Ostrom, P., Grandy, A., Huizinga, K., and Robertson, G.: Isotopologue effects during N_2O reduction in soils and in pure cultures of denitrifiers, J. Geophys. Res., 112, G02005, https://doi.org/10.1029/2006jg000287, 2007.

Ostrom, N. E., Gandhi, H., Coplen, T. B., Toyoda, S., Böhlke, J. K., Brand, W. A., Casciotti, K. L., Dyckmans, J., Giesemann, A., Mohn, J., Well, R., Yu, L., and Yoshida, N.: Preliminary assessment of stable nitrogen and oxygen isotopic composition of USGS51 and USGS52 nitrous oxide reference gases and perspectives on calibration needs, Rapid Commun. Mass Sp., 32, 1207–1214, https://doi.org/10.1002/rcm.8157, 2018.

Prins, R.: On the structure of γ-Al_2O_3, J. Catal., 392, 336–346, https://doi.org/10.1016/j.jcat.2020.10.010, 2020.

Robertson, P. J., Scurrell, M. S., and Kembell, C.: Exchange of Alkanes with Deuterium over γ-Alumina, J. Chem. Soc. Farad. T. 1, 71, 903–912, https://doi.org/10.1039/F19757100903, 1975.

Sadiek, I., Hjältén, A., Friedrichs, G., and Foltynowicz, A.: HNO Dimerization as a Chemical Reference Standard for N_2O Isotopomer Ratio: Ab Initio Calculations, Formation Kinetics, and Frequency Comb Spectroscopy, J. Am. Chem. Soc., https://doi.org/10.1021/jacs.5c09983, 2025.

Schlagin, J., Dinu, D., Liedl, K. R., Stolzenburg, D., Grothe, H., and Mohn, J.: Towards a calibration-free analysis of ^{15}N site preference in N_2O reference materials using matrix-isolation infrared spectroscopy, EGU General Assembly 2025, Vienna, Austria, 27 Apr–2 May 2025, EGU25-11143, https://doi.org/10.5194/egusphere-egu25-11143, 2025.

Schmidt, J. A. and Johnson, M. S.: Clumped isotope perturbation in tropospheric nitrous oxide from stratospheric photolysis, Geophys. Res. Lett., 42, 3546–3552, https://doi.org/10.1002/2015GL063102, 2015.

Stolper, D., Sessions, A. L., Ferreira, A. A., Neto, E. V. S., Schimmelmann, A., Shusta, S. S., Valentine, D. L., and Eiler, J. M.: Combined ^{13}C–D and D–D clumping in methane: Methods and preliminary results, Geochim. Cosmochim. Ac., 126, 169–191, https://doi.org/10.1016/j.gca.2013.10.045, 2014.

Tian, H., Xu, R., Canadell, J. G., Thompson, R. L., Winiwarter, W., Suntharalingam, P., Davidson, E. A., Ciais, P., Jackson, R. B., Janssens-Maenhout, G., Prather, M. J., Regnier, P., Pan, N., Pan, S., Peters, G. P., Shi, H., Tubiello, F. N., Zaehle, S., Zhou, F., Arneth, A., Battaglia, G., Berthet, S., Bopp, L., Bouwman, A. F., Buitenhuis, E. T., Chang, J., Chipperfield, M. P., Dangal, S. R. S., Dlugokencky, E., Elkins, J. W., Eyre, B. D., Fu, B., Hall, B., Ito, A., Joos, F., Krummel, P. B., Landolfi, A., Laruelle, G. G., Lauerwald, R., Li, W., Lienert, S., Maavara, T., MacLeod, M., Millet, D. B., Olin, S., Patra, P. K., Prinn, R. G., Raymond, P. A., Ruiz, D. J., Van Der Werf, G. R., Vuichard, N., Wang, J., Weiss, R. F., Wells, K. C., Wilson, C., Yang, J., and Yao, Y.: A comprehensive quantification of global nitrous oxide sources and sinks, Nature, 586, 248–256, https://doi.org/10.1038/s41586-020-2780-0, 2020.

Toyoda, S. and Yoshida, N.: Determination of Nitrogen Isotopomers of Nitrous Oxide on a Modified Isotope Ratio Mass Spectrometer, Anal. Chem., 71, 4711–4718, https://doi.org/10.1021/ac9904563, 1999.

Turner, A. C., Korol, R., Eldridge, D. L., Bill, M., Conrad, M. E., Miller, T. F., and Stolper, D. A.: Experimental and theoretical determinations of hydrogen isotopic equilibrium in the system CH_4–H_2–H_2O from 3 to 200 °C, Geochim. Cosmochim. Ac., 314, 223–269, https://doi.org/10.1016/j.gca.2021.04.026, 2021.

Tuzson, B., Mohn, J., Zeeman, M. J., Werner, R. A., Eugster, W., Zahniser, M. S., Nelson, D. D., McManus, J. B., and Emmenegger, L.: High precision and continuous field measurements of $\delta^{13}C$ and $\delta^{18}O$ in carbon dioxide with a cryogen-free QCLAS, Appl. Phys. B-Lasers O., 92, 451, https://doi.org/10.1007/s00340-008-3085-4, 2008.

Urey, H. C.: The thermodynamic properties of isotopic substances, J. Chem. Soc., 562–581, https://doi.org/10.1039/JR9470000562, 1947.

Urey, H. C. and Rittenberg, D.: Some Thermodynamic Properties of the H^1H^2, H^2H^2 Molecules and Compounds Containing the H_2 Atom, J. Chem. Phys., 1, 137–143, https://doi.org/10.1063/1.1749265, 1933.

Waechter, H., Mohn, J., Tuzson, B., Emmenegger, L., and Sigrist, M. W.: Determination of N_2O isotopomers with quantum cascade laser based absorption spectroscopy, Opt. Express, 16, 9239, https://doi.org/10.1364/OE.16.009239, 2008.

Wang, D. T., Sattler, A., Paccagnini, M., and Chen, F. G.: Method for calibrating methane clumped isotope measurements via catalytic equilibration of methane isotopologues on γ-alumina, Rapid Commun. Mass Sp., 34, e8555, https://doi.org/10.1002/rcm.8555, 2020a.

Wang, Z., Schauble, E. A., and Eiler, J. M.: Equilibrium thermodynamics of multiply substituted isotopologues of molecular gases, Geochim. Cosmochim. Ac., 68, 4779–4797, https://doi.org/10.1016/j.gca.2004.05.039, 2004.

Wang, Z., Nelson, D. D., Dettman, D. L., McManus, J. B., Quade, J., Huntington, K. W., Schauer, A. J., and Sakai, S.: Rapid and Precise Analysis of Carbon Dioxide Clumped Isotopic Composition by Tunable Infrared Laser Differential Spectroscopy, Anal. Chem., 92, 2034–2042, https://doi.org/10.1021/acs.analchem.9b04466, 2020b.

Webb, M. A. and Miller, T. F.: Position-Specific and Clumped Stable Isotope Studies: Comparison of the Urey and Path-Integral Approaches for Carbon Dioxide, Nitrous Oxide, Methane, and Propane, J. Phys. Chem. A, 118, 467–474, https://doi.org/10.1021/jp411134v, 2014.

Werle, P.: Accuracy and precision of laser spectrometers for trace gas sensing in the presence of optical fringes and atmospheric turbulence, Appl. Phys. B-Lasers O., 102, 313–329, https://doi.org/10.1007/s00340-010-4165-9, 2011.

Werle, P., Mücke, R., and Slemr, F.: The limits of signal averaging in atmospheric trace-gas monitoring by tunable diode-laser absorption spectroscopy (TDLAS), Appl. Phys. B-Lasers O., 57, 131–139, https://doi.org/10.1007/BF00425997, 1993.

Westley, M., Popp, B., and Rust, T.: The calibration of the intramolecular nitrogen isotope distribution in nitrous oxide measured by isotope ratio mass spectrometry, Rapid Commun. Mass Sp., 21, 391–405, https://doi.org/10.1002/rcm.2828, 2007.

Yeung, L. Y.: Combinatorial effects on clumped isotopes and their significance in biogeochemistry, Geochim. Cosmochim. Ac., 172, 22–38, https://doi.org/10.1016/j.gca.2015.09.020, 2016.

Yu, L., Harris, E., Lewicka-Szczebak, D., Barthel, M., Blomberg, M. R. A., Harris, S. J., Johnson, M. S., Lehmann, M. F., Liisberg, J., Müller, C., Ostrom, N. E., Six, J., Toyoda, S., Yoshida, N., and Mohn, J.: What can we learn from N_2O isotope data? – Analytics, processes and modelling, Rapid Commun. Mass Sp., 34, e8858, https://doi.org/10.1002/rcm.8858, 2020.

Zhang, N., Prokhorov, I., Kueter, N., Li, G., Tuzson, B., Magyar, P. M., Ebert, V., Sivan, M., Nakagawa, M., Gilbert, A., Ueno, Y., Yoshida, N., Röckmann, T., Bernasconi, S. M., Emmenegger, L., and Mohn, J.: Rapid High-Sensitivity Analysis of Methane Clumped Isotopes ($\Delta^{13}CH_3D$ and $\Delta^{12}CH_2D_2$) Using Mid-Infrared Laser Spectroscopy, Anal. Chem., 97, 1291–1299, https://doi.org/10.1021/acs.analchem.4c05406, 2025.